Electronic Supplementary Material (ESI) for Journal of Materials Chemistry C.

Supporting Information

Guest-controlled polymorphism and exceptionally marked bi-stability in a spin crossover 3D porous amino-functionalized coordination polymer

Alejandro Orellana-Silla,[a] Manuel Meneses-Sánchez,[a] Rubén Turo-Cortés,[a] Víctor Rubio-Giménez,[b] Giel Arnauts,[b] M. Carmen Muñoz,[c] Rob Ameloot,[b] Carlos Bartual-Murgui*[a] and José Antonio Real*[a]

[a]Departamento de Química Inorgánica, Instituto de Ciencia Molecular (ICMol), Universidad de Valencia, C/ Catedrático José Beltrán Martínez, 2, 46980 Paterna, Valencia, Spain.
[b]Centre for Membrane Separations, Adsorption, Catalysis and Spectroscopy (cMACS), Katholieke Universiteit Leuven, Celestijnenlaan 200F, 3001 Leuven, Belgium
[c]Departamento de Fisica Aplicada, Universitat Politècnica de València, Camino de Vera s/n, 46022 Valencia, Spain

Contents

Page

Experimental section

Synthesis

Iron(II) tetrafluoroborate hexahydrate, potassium dicyanoaurate(I), Iron(II) chloride tetrahydrate, n-tetrabuthylammonium bromide were obtained from commercial sources and used as received without further purification. Tetra-n-butylammonium dicyanoaurate(I), the ligand 2,5-di(pyridin-4-yl)aniline (dpyan) were synthesized according to methods described in the literature. [1, 2]

Fresh crystals of compounds **1·guest** were prepared with yields of 60-70% by liquid-liquid slow diffusion in H-shaped tubes (**1·MeOH**, **1·EtOH** and **1·NO_2Bz**) or test tubes (**1·H_2O·MeOH**). For the synthesis of **1·MeOH**, **1·NO_2Bz** and **1·H_2O·MeOH**, square-plate yellow crystals were obtained within two weeks using as precursors dpyan, $Fe(BF_4)_2 \cdot 6H_2O$ and $K[Au(CN)_2]$. For the synthesis of compound **1·EtOH**, $FeCl_2 \cdot 4H_2O$ and $TBA[Au(CN)_2]$ (TBA = tetrabutylammonium) were used for better yields. Square-plate yellow crystals were obtained after three weeks.

As a general procedure for the synthesis of compounds **1·MeOH**, **1·EtOH** and **1·NO_2Bz**, 0.1 mmol of the iron salt was introduced in one side of the H-shaped tube and 0.2 mmol of dpyan and 0.2 mmol of the gold salt in the other side. Methanol, ethanol, or a mixture of methanol/nitrobenzene (8:2) were respectively used for filling the H-shaped tubes, which were subsequently sealed with parafilm and left undisturbed at room temperature. For obtaining compound **1·H_2O·MeOH**, 0.1 mmol of $Fe(BF_4)_2 \cdot 6H_2O$ in 2 mL of water/methanol (1:2), 5 mL of water/methanol (1:4) and 0.2 mmol of dpyan and 0.2 mmol $K[Au(CN)_2]$ in 2 mL of methanol were successively layered in test tubes, which were subsequently sealed with parafilm and left undisturbed at room temperature. Solvent free compound **1·ø** was obtained from any of the **1·MeOH**, **1·EtOH** or **1·H_2O·MeOH** solvates by heating at 400 K for 10 minutes or by heating **1·NO_2Bz** at 473 K for 1 h. The elemental analysis was performed just for **1·NO_2Bz** and **1·ø** which were stable in normal conditions without loss of solvents. Anal. Calculated for **1·NO_2Bz** [$C_{26}H_{18}FeN_8O_2Au_2$ (924.5) (%)]: C 33.79, H 1.96, N 12.12. Found (%): C 33.42, H 2.19, N 12.32; Anal. Calculated for **1·ø** [$C_{20}H_{13}FeN_7O_2Au_2$(801.14) (%)]: C 39.98, H 1.64, N 12.24. Found (%): C 39.56, H 1.51, N 12.11.

Physical Measurements.

Magnetic Measurements. Variable temperature magnetic susceptibility data were recorded in sweep mode at a rate of 2 K/min with a Quantum Design MPMS2 SQUID magnetometer equipped with a 7 T magnet, operating at 1 T and at temperatures 50-400 K. Experimental susceptibilities were corrected for diamagnetism of the constituent atoms using Pascal's constants.

Single Crystal X-ray Diffraction. Single-crystal X-ray data were collected on an Oxford Diffraction Supernova diffractometer using graphite monochromated MoKα radiation (λ = 0.71073 Å). A multiscan absorption correction was performed. The structures were solved by direct methods using SHELXS-2014 and refined by fullmatrix least-squares on F^2 using SHELXL-2014.[3] Non-hydrogen atoms were refined anisotropically and hydrogen atoms were placed in calculated positions refined using idealized geometries (riding model) and assigned fixed isotropic displacement parameters. All details can be found in CCDCs 2277962 (**1·NO2Bz**_120 K), 2277963 (**1·NO_2Bz**_250K), 2277964 (**1·EtOH**_120K), 2277965 (**1·EtOH**_200 K), 2277966 (**1·H_2O·MeOH**_120 K) and 2277967 (**1·H2O·MeOH**_260 K), which contain the supplementary crystallographic data for this article. These data can be obtained free of charge from The Cambridge Crystallographic Data Centre via www.ccdc.cam. ac.uk/data_request/cif.

Powder X-ray diffraction measurements were performed on a PANalytical Empyrean X-ray powder diffractometer (monochromatic CuKα radiation) in capillary measurement mode.

In situ powder X-ray diffraction (PXRD). Temperature dependent measurement were performed in a Malvern PANalytical Empyrean diffractometer equipped with a TTK-600 nonambient chamber (Anton Paar) with Kapton windows connected to a two-stage rotary vane vacuum pump. Diffractograms were collected in reflection geometry with a step size of 0.0131° and a counting time of 75 seconds. A PIXcel3D solid-state detector in scanning mode and a Cu anode (Cu Kα1 = 1.5406 Å; Cu Kα2 = 1.5444 Å) operating at 45 kV and 40 mA were employed together with 0.02° Soller slits of and ¼ divergence and anti-scatter slits. Powder samples were carefully grinded and loaded into a sample holder inside the TTK-600 non-ambient chamber and heated under dynamic vacuum (~10^{-3} mbar).

Elemental analyses (C, H, and N) were performed with a CE Instruments EA 1110 CHNS Elemental analyzer.

TGA experiments were carried out with a TA instruments TGA550 device equipped with a Pt/Rh oven (Tmax = 1000°C).

Mass spectrometry-thermogravimetric analysis (MS-TGA). MS-TGA measurements were performed on a Netzsch STA 449F3 (TGA) coupled with 3idden HPR20 QIC-EGA (MS). The heating rate was 3 °C min^{-1} under N_2 atmosphere. M/Z of 17 and 37, corresponding to water and methanol, respectively, were recorded during heating.

References

1. W. R. Mason, H. B. Gray, Electronic Structures of Square-Planar Complexes. *J. Am. Chem. Soc*. **1968**, *90*, 5721-5729.
2. J. T. Culp, C. Madden, K. Kauffman, F. Shi, C. Matranga, Screening Hofmann Compounds as CO2 Sorbents: Nontraditional Synthetic Route to Over 40 Different Pore-Functionalized and Flexible Pillared Cyanonickelates. *Inorg. Chem.* **2013**, *52*, 4205-4216.
3. a) G. M. Sheldrick, *Acta Crystallogr., Sect. A*: Found. Crystallogr. 2008, 64, 112; b) G. M. Sheldrick, SHELXL-2014, University of Göttingen, 2014.

Figure S1. TGA of freshly air-dried samples of compounds a) **1·MeOH**, b) **1·EtOH**, and c) **1·NO₂Bz**.

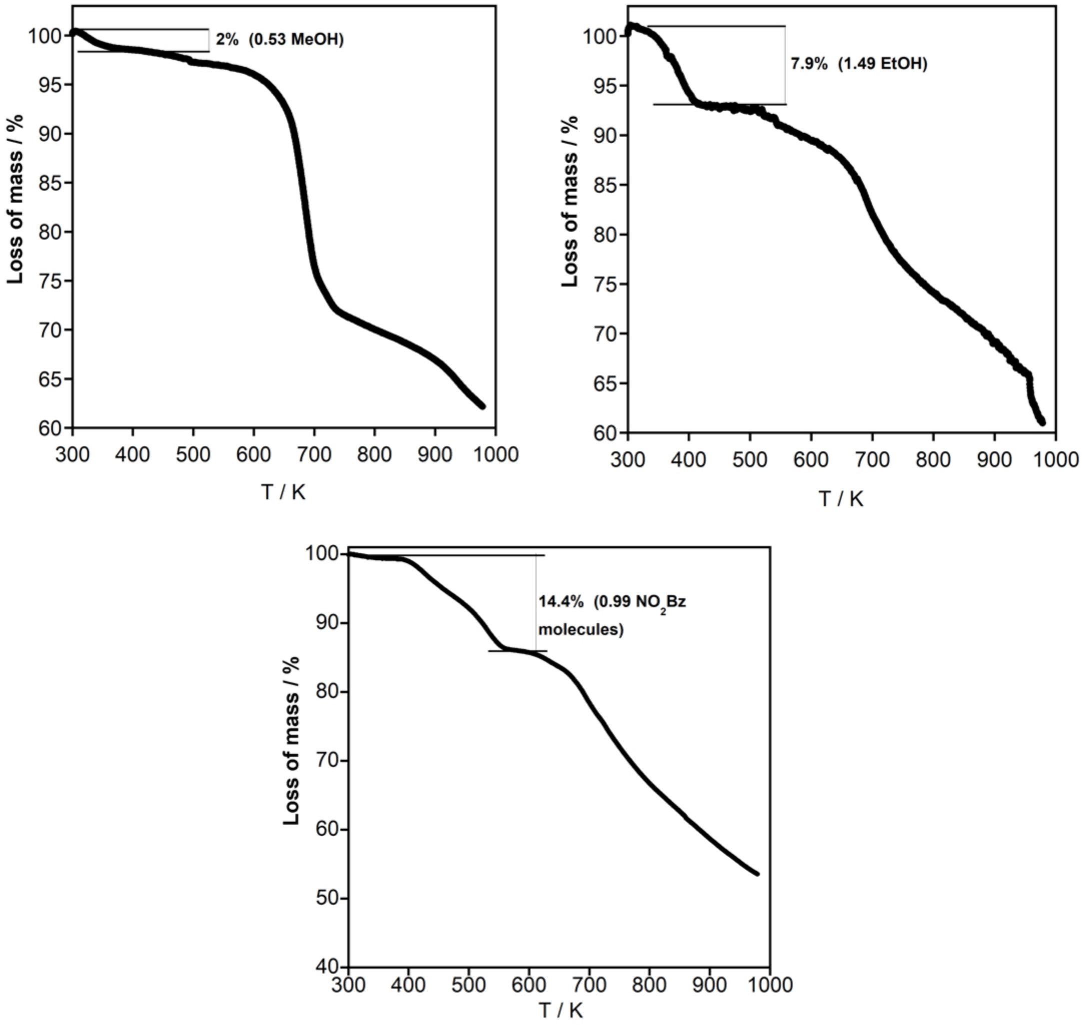

Figure S2. TGA-mass measurements of a sample of 1·H2O·MeOH just after removing from the mother liquor (left) and three weeks after exposed to air (right).

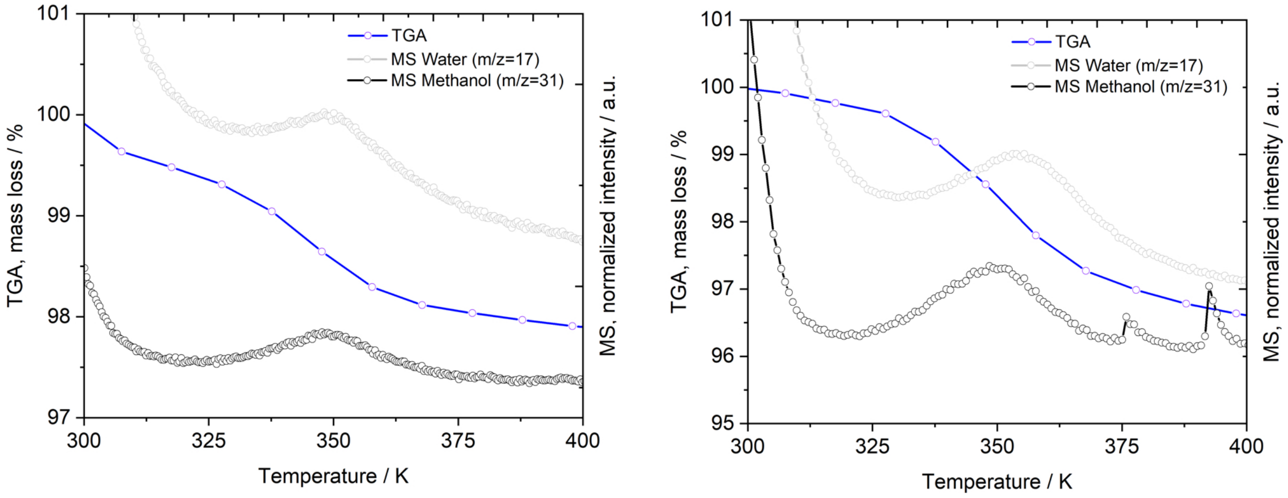

Figure S3. TGA of compounds **1·xNO$_2$Bz** with different nitrobenzene contents obtained from controlled heating of the original **1·NO$_2$Bz** (with 0.99 molecules of nitrobenzene)

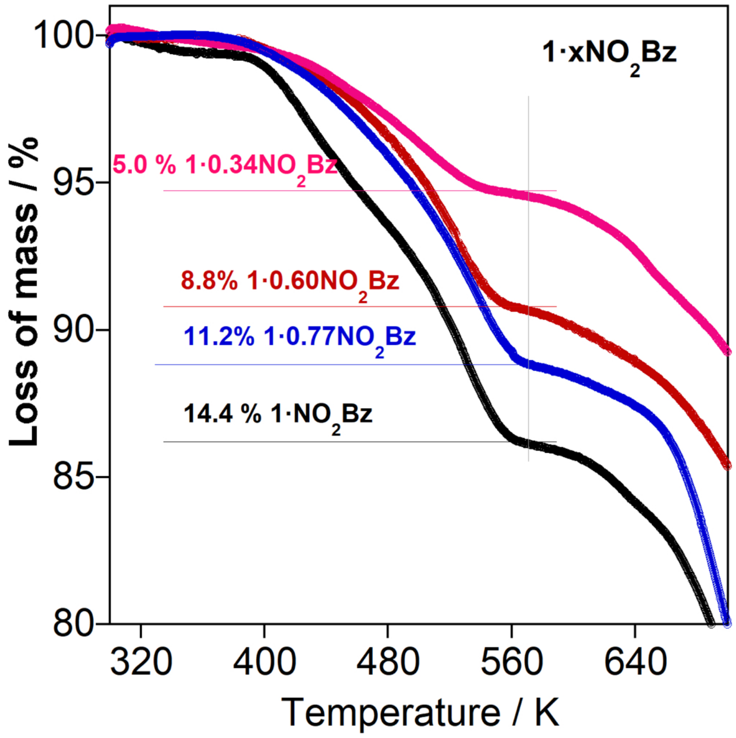

Figure S4. TGA of a desorbed sample of **1·MeOH** that was exposed to air for three days.

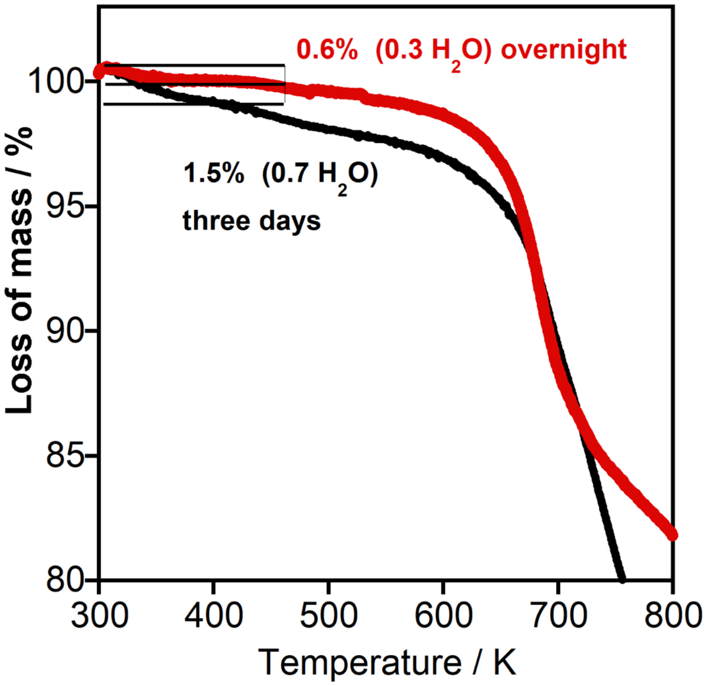

Table S1. Crystal data for **1·NO_2Bz and 1·H_2O·MeOH** (orthorhombic phase).

	1·NO_2Bz		**1·H_2O·MeOH**	
Empirical formula	$C_{26}H_{15}N_8O_2Au_2Fe$	$C_{26}H_{17}N_8O_2Au_2Fe$	$C_{21}H_{10}N_7O_2Au_2Fe$	
Mr	921.24	923.26	842.14	
Crystal system	orthorhombic			
Space group	*Cmma*			
a (Å)	13.2345(4)	13.2993(5)	12.2789(5)	12.1936(4)
b (Å)	15.3279(4)	16.1917(5)	15.9530(8)	16.8942(5)
c (Å)	15.4071(5)	15.7387(4)	15.4253(7)	15.7796(5)
V (Å^3)	3125.4(2)	3389.1(2)	3021.6(2)	3250.6(3)
Z	4			
T (K)	120	250	120	260
D_c (mg cm^{-3})	1.958	1.809	1.851	1.721
F(000)	1708	1716	1540	1540
μ (Mo-K$_\alpha$) (mm^{-1})	9.857	9.090	10.185	20.367
Crystal size (mm)	0.05x0.20x0.20		0.03x0.20x0.20	
No. of total reflections	1695	1869	2523	1779
No. of reflections [$I>2\sigma(I)$]	1339	1474	1450	1543
R [$I>2\sigma(I)$]	0.0461	0.0414	0.0486	0.0520
wR [$I>2\sigma(I)$]	0.1130	0.1196	0.1264	0.1617
S	1.115	1.074	1.095	1.078

$R = \Sigma\,||Fo| - |Fc||\,/\,\Sigma\,|Fo|$; $wR = [\,\Sigma\,[w(Fo^2 - Fc^2)^2]\,/\,\Sigma\,[w(Fo^2)^2]]^{1/2}$.
$w = 1/\,[\sigma^2(Fo^2) + (\mathrm{m}\,P)^2 + \mathrm{n}\,P]$ where $P = (Fo^2 + 2Fc^2)\,/\,3$;
m = 0.0436 (**1**), 0.0683 (**2**), 0.0613 (**3**), 0.0889 (**4**), and 0.1176 (**5**);
n = 63.2353 (**1**), 12.0021 (**2**), 67.8767 (**3**), 7.4363 (**4**), and 5.2882 (**5**)

Table S2. Selected bond lengths [Å] and angles [°].

	1·NO_2Bz		**1·H_2O·MeOH**	
Fe-N(1)	1.939(7)	2.135(6)	1.936(7)	2.135(6)
Fe-N(2)	1.986(14)	2.184(12)	2.04(2)	2.173(12)
Fe-N(3)	1.989(13)	2.169(13)	2.01(2)	2.173(10)
Au(Ag)-C(1)	1.992(9)	1.983(8)	1.977(8)	1.974(7)
N(1)-Fe-N(2)	90.2(2)	90.5(2)	89.5(2)	89.79(14)
N(1)-Fe-N(3)	89.8(2)	89.5(2)	90.5(2)	90.21(14)
C(1)-Au(Ag)-C(1)	177.7(4)	177.3(4)	177.4(5)	175.9(3)

Table S3. Crystal data for **1·EtOH** (monoclinic phase).

	1·EtOH	
Empirical formula	$C_{23}H_{12}N_7O_{1.5}Au_2Fe$	
*M*r	860.18	
Crystal system	monoclinic	
Space group	*P*2/*c*	
a (Å)	15.4088(5)	15.7586(4)
b (Å)	10.4132(4)	10.0533(3)
c (Å)	16.8957(5)	17.8234(4)
β (°)	91.220(3)	92.083(2)
V (Å^3)	2710.4(2)	2821.82(13)
Z	4	
T (K)	120	200
D_c (mg cm^{-3})	2.108	2.025
F(000)	1580	1580
μ (Mo-K$_\alpha$) (mm^{-1})	24.431	23.466
Crystal size (mm)	0.02x0.10x0.15	
No. of total reflections	5401	5644
No. of reflections [$I>2\sigma(I)$]	3827	4157
R [$I>2\sigma(I)$]	0.0637	0.0516
wR [$I>2\sigma(I)$]	0.1840	0.1380
S	1.033	0.992

$R = \Sigma ||Fo| - |Fc|| / \Sigma |Fo|$; $wR = [\Sigma [w(Fo^2 - Fc^2)^2] / \Sigma [w(Fo^2)^2]]^{1/2}$.
$w = 1/ [\sigma^2(Fo^2) + (m\ P)^2 + n\ P]$ where $P = (Fo^2 + 2Fc^2) / 3$;
m = 0.1609 (**1**), and 0.1131 (**2**);
n = 0.0000 (**1**), and 0.0000 (**2**)

Table S4. Selected bond lengths [Å] and angles [°] for **1·EtOH**.

	1·EtOH	
Fe-N(1)	1.928(11)	2.156(7)
Fe-N(2)	1.931(11)	2.143(7)
Fe-N(3)	1.950(12)	2.179(7)
Fe-N(4)	1.916(11)	2.141(7)
Fe-N(5)	1.975(11)	2.186(7)
Fe-N(6)	1.981(10)	2.195(7)
Au(1)-C(1)	1.978(11)	2.002(8)
Au(1)-C(4)	1.993(13)	2.003(7)
Au(2)-C(2)	2.000(11)	1.987(7)
Au(2)-C(3)	1.973(11)	2.007(8)
N(1)-Fe-N(2)	85.5(4)	85.8(3)
N(1)-Fe-N(3)	178.0(4)	177.0(3)
N(1)-Fe-N(4)	94.0(4)	94.0(3)
N(1)-Fe-N(5)	91.0(4)	91.6(3)
N(1)-Fe-N(6)	88.5(4)	88.5(3)
N(2)-Fe-N(3)	94.8(5)	93.6(3)
N(2)-Fe-N(4)	178.9(4)	179.2(3)
N(2)-Fe-N(5)	90.3(4)	90.6(3)
N(2)-Fe-N(6)	90.3(4)	89.2(3)
N(3)-Fe-N(4)	85.8(4)	86.6(3)
N(3)-Fe-N(5)	91.0(4)	91.3(3)
N(3)-Fe-N(6)	89.5(4)	88.5(3)
N(4)-Fe-N(5)	88.7(4)	90.2(3)
N(4)-Fe-N(6)	90.7(4)	90.0(3)
N(5)-Fe-N(6)	179.2(4)	179.8(3)
C(1)-Au(1)-C(4)	176.1(6)	175.2(4)
C(2)-Au(2)-C(3)	175.7(6)	175.7(4)

Figure S5. Perspective views of the structures of **1·NO₂Bz** and **1·H₂O·MeOH** showing the electronic density found in the pores and ascribed to the respective included guest. Note that whereas the nitrobenzene electronic residue is spread within the whole available void space of the pore, it is limited to specific positions for the water/methanol guests.

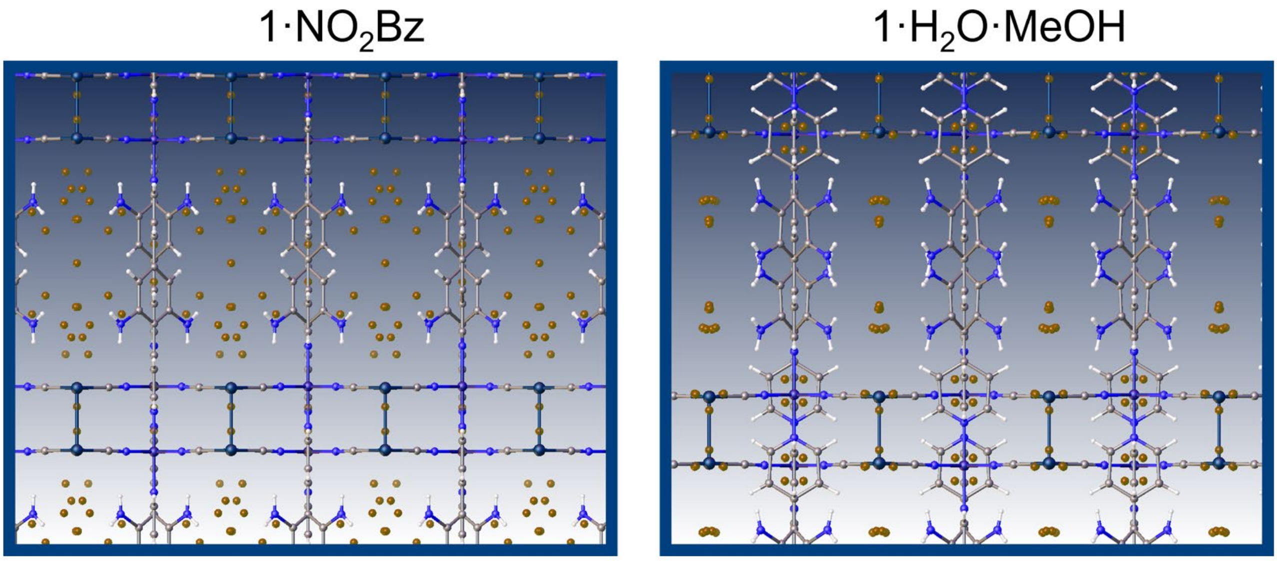

Figure S6. Fragment of the structure of **1·EtOH** highlighting the short contacts between aromatic rings of the dpyan ligands belonging to each interpenetrated network (see table S5).

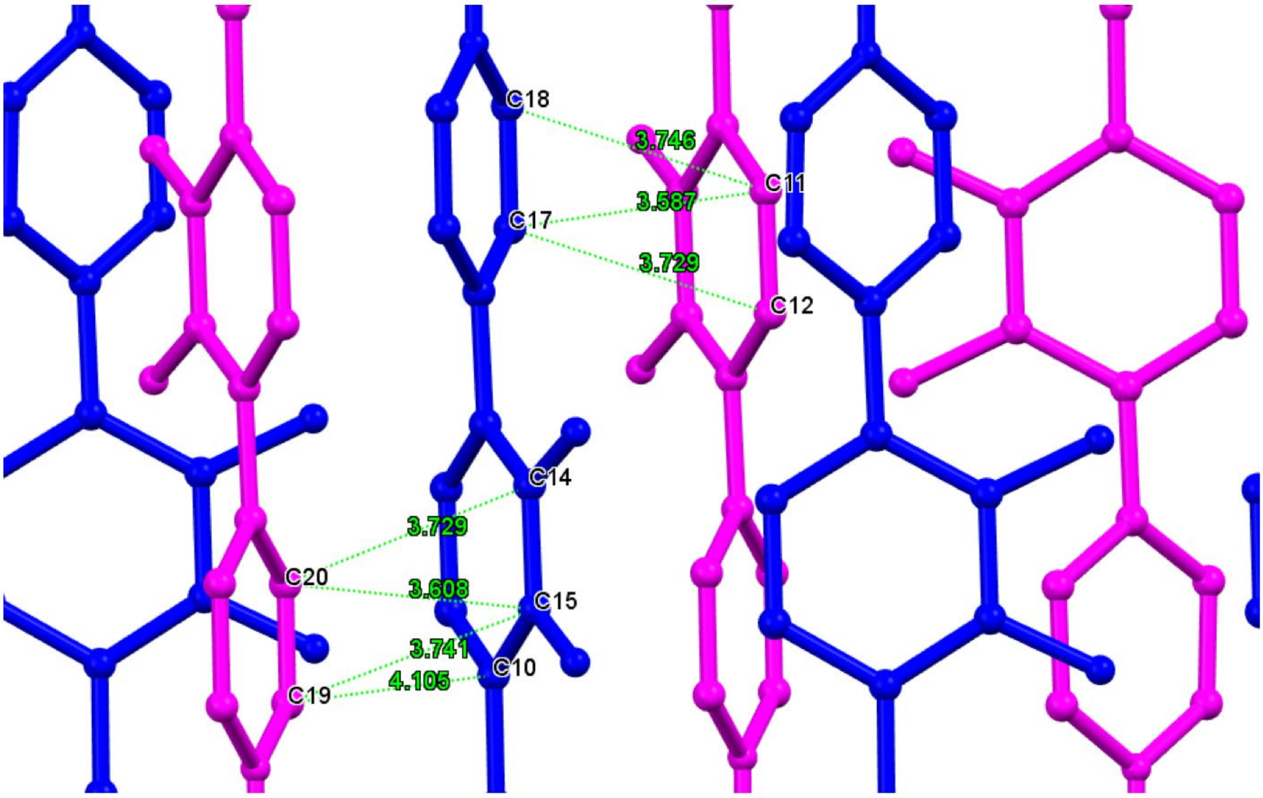

Table S5. List of C···C short contacts found between the interpenetrated apical dpyan ligands in compound **1·EtOH**.

Contact	**Distance (Å)**
C17···C11	3.5874
C10···C19	4.1050
C12···C17	3.7293
C15···C19	3.7411
C20···C14	3.7294
C11···C18	3.7457
C15···C20	3.6076

Figure S7. Fragment of the structure of compound **1·EtOH** showing the multiple H-bond interactions (see **Table S6**) operating between the ethanol molecules and the amino groups of the host framework.

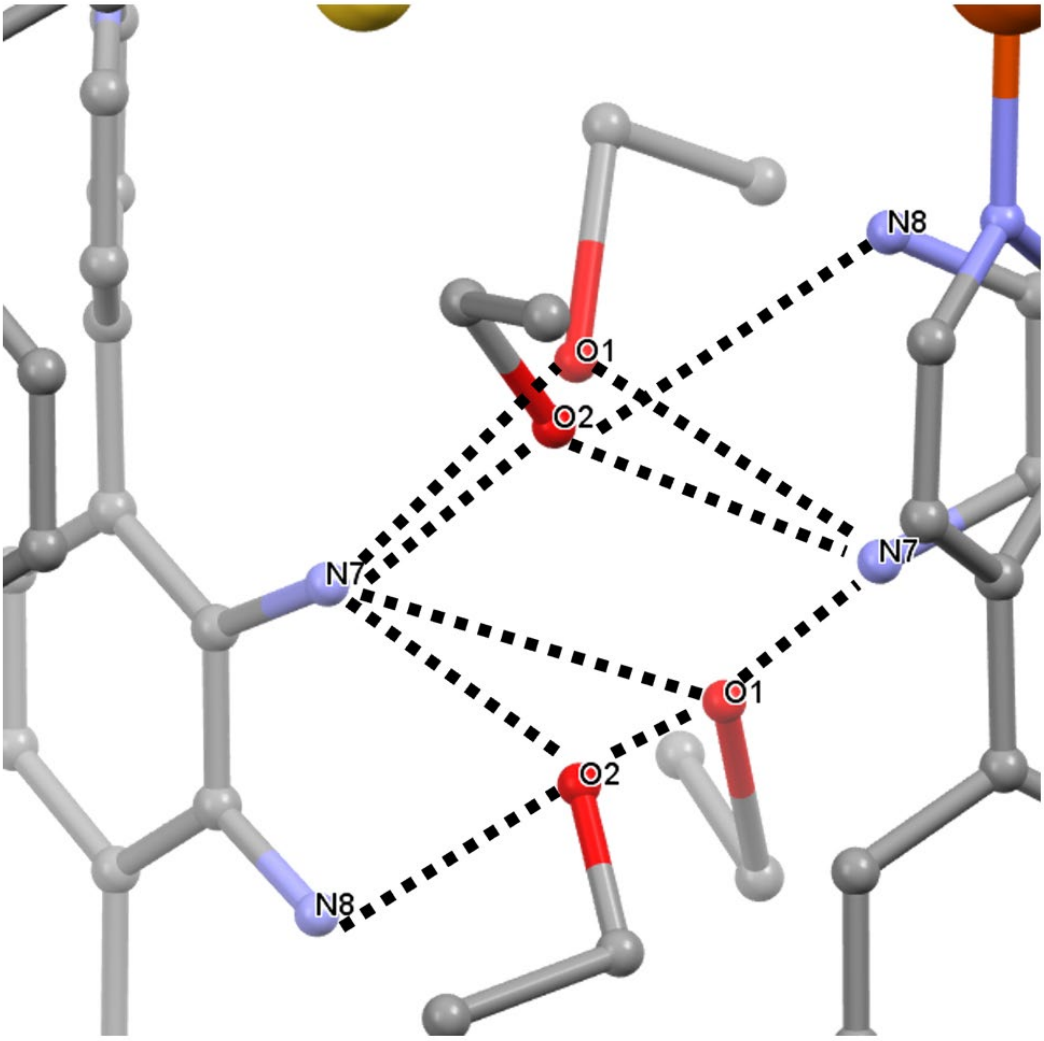

Table S6. List of O···N and O···O H-bonds found between the ethanol molecules and the amine groups of the host network in **1·EtOH**.

Contact	distance (Å)
O2··· N7	2.859
O1 ···N7	2.609
O2··· N7	2.788
O1 ···N7	3.276
O2···N8	2.956
O2···N8	2.860
O2··· O1	2.518

Figure S8. TGA performed for a sample of **1·NO$_2$Bz** after being heated under successive thermal cycles from 350 to 380 K inside the powder X-ray diffractometer chamber.

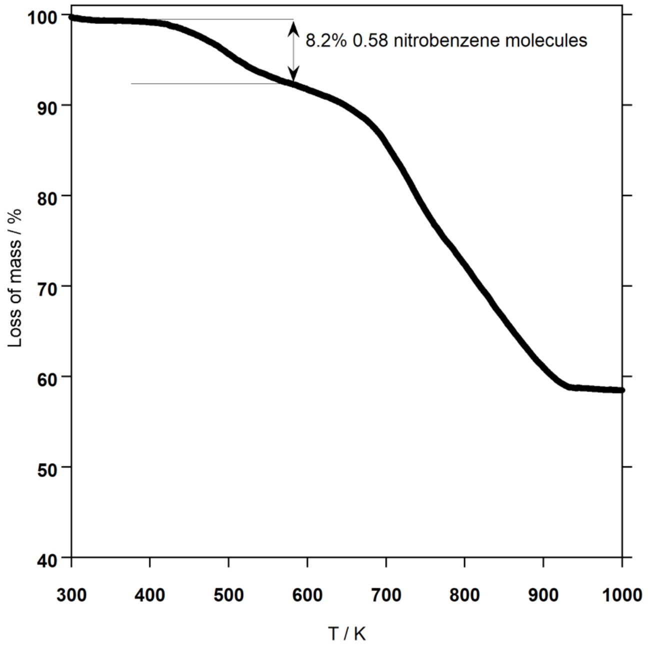

Figure S9. PXRD patterns of samples of **1·ø** redispersed in nitrobenzene (top), methanol/water (1:1) (middle) for a week. The pattern of the empty **1·ø** sample (bottom) is also showed for comparison.

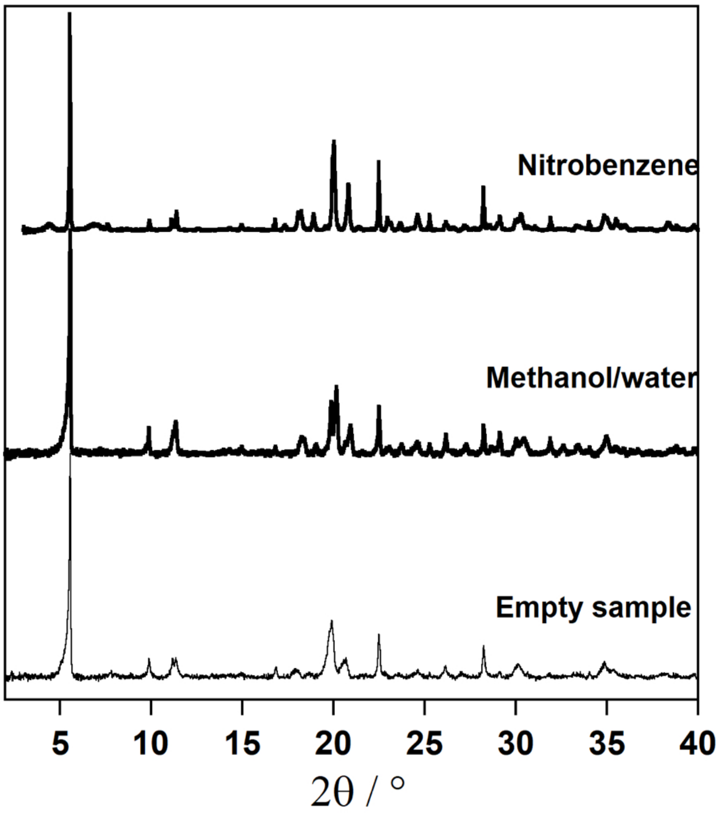

Figure S10. Thermal dependence of χ_MT for **1·H₂O·MeOH** after the sample is removed from the mother liquor and exposed to air for 1 day (blue plot) and 1 week (red plot).

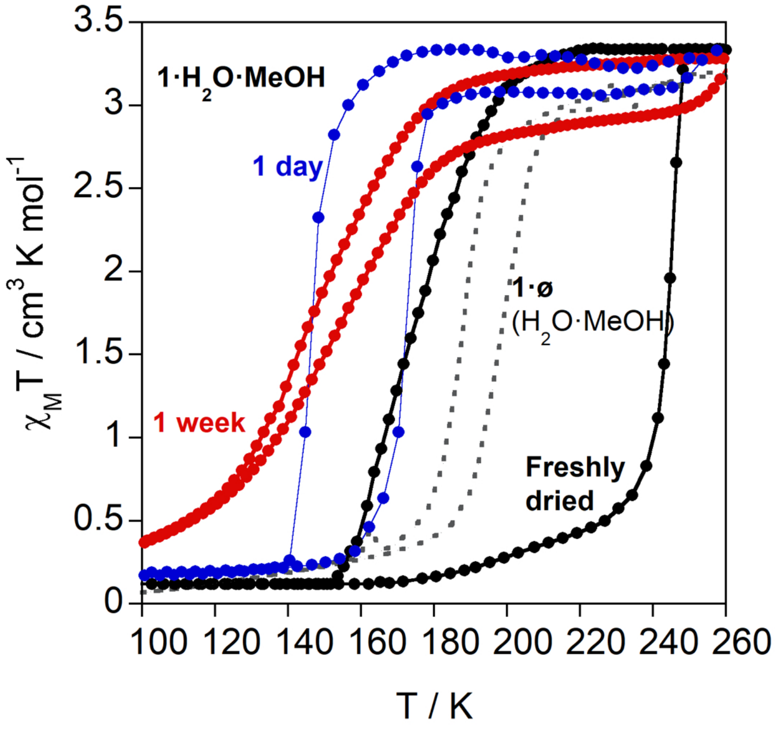

Figure S11. Thermal dependence of χ_MT of a sample of **1·0.77NO₂Bz** just after being obtained (in red) and one month after leaving it under ambient conditions (in black).

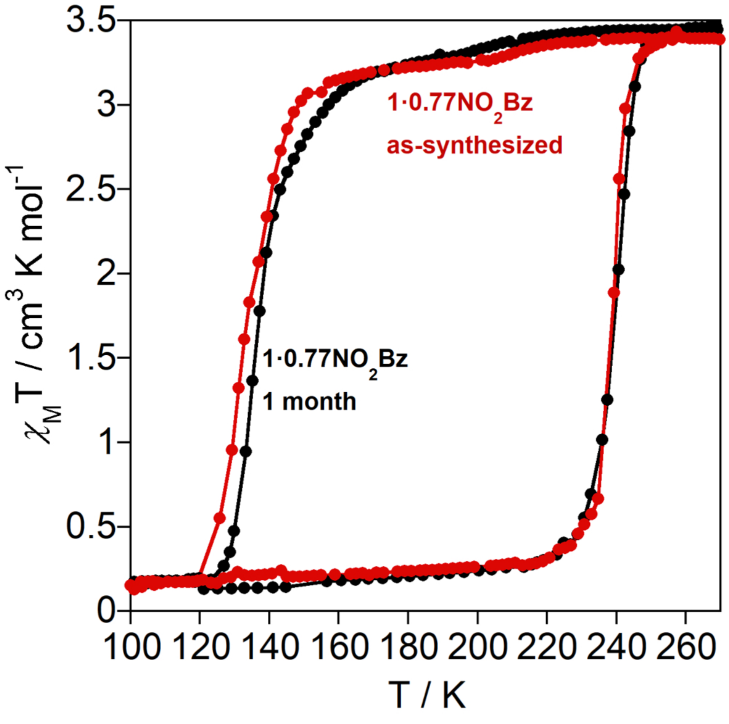

Figure S12. Thermal dependence of $\chi_M T$ at different temperature scan rates for a sample of **1·0.72NO$_2$Bz**.

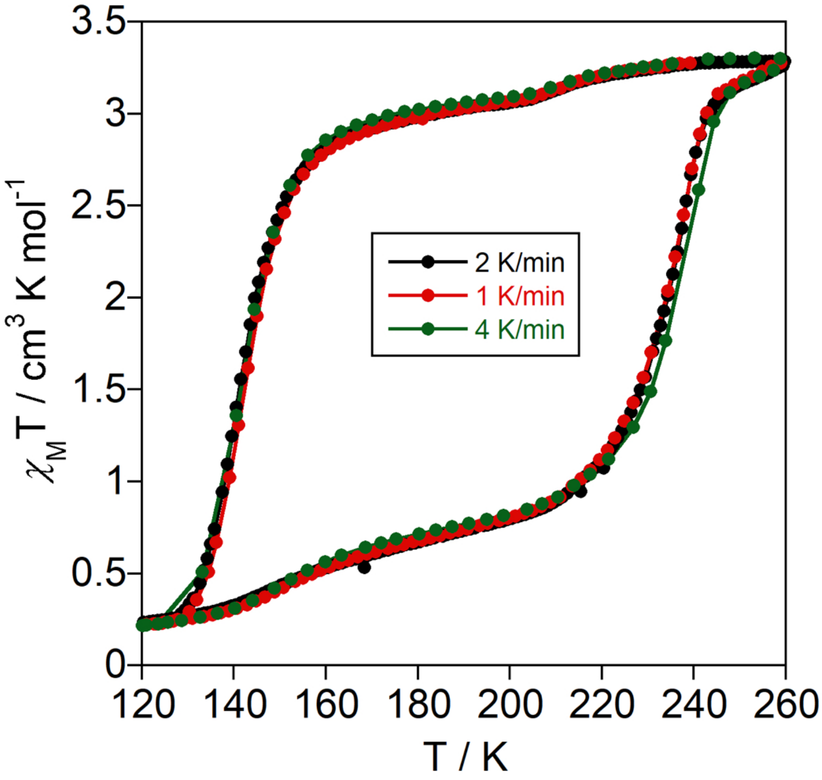

Figure S13. TGA performed for a sample of **1·NO$_2$Bz** after being heated under successive thermal cycles from 350 to 380 K inside the SQUID chamber.

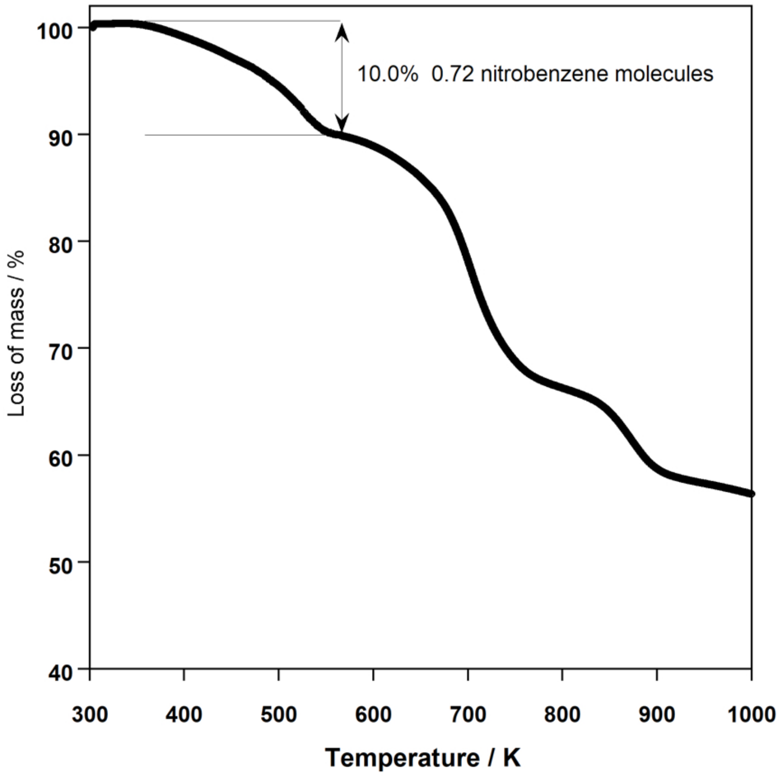

Figure S14. Thermal dependence of $\chi_M T$ for a sample of **1·ø** before (red plot) and after (black plot) re-adsorbing 0.7 molecules of water under ambient conditions for three days.

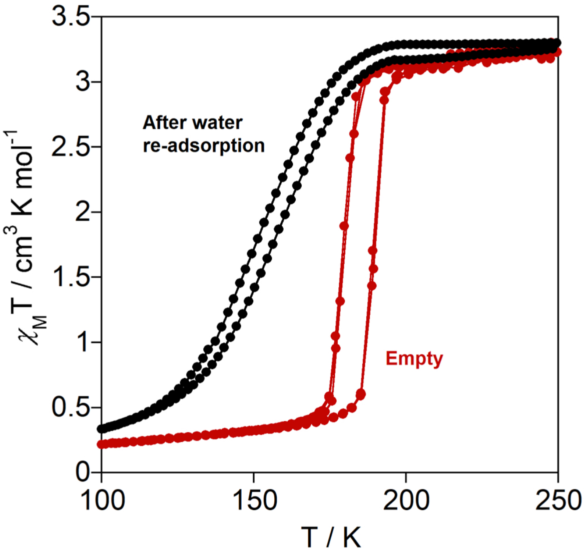

Figure S15. Thermal dependence of the $\chi_M T$ for **1·ø** (empty) and for a sample of **1·ø** redispersed in a) methanol, b) ethanol and c) nitrobenzene, measured in situ throughout several $\chi_M T$ vs T cycles until curve stabilization (the stabilized or "saturated" curves are depicted in black). Blue plots correspond to intermediate $\chi_M T$ vs T cycles before stabilization. Figure d) include the saturated curves for all guests for comparison.